

A Milky Way mass model for isolated simulations

J. A. SELLWOOD¹

¹*Steward Observatory, University of Arizona, 933 Cherry Avenue, Tucson, AZ 85722, USA*

ABSTRACT

This paper presents an equilibrium model of a Milky Way-like spiral galaxy that supports open, mostly 2- and 3-arm spiral patterns but does not form a bar. It is suggested as a more realistic alternative model to that employed by the AGORA collaboration; their model has a much lower disk mass and therefore forms only multi-arm spiral patterns. This improved model should enable simulations that test star-formation and feedback models in a more realistic isolated galaxy. Three versions of the same model having 2.1×10^5 , 2.1×10^6 , and 2.1×10^7 particles are available for download.

1. THE AGORA MODEL

As an offshoot from the on-going AGORA project (*e.g.* Kim et al. 2014; Jung et al. 2025), Kim et al. (2016) constructed an equilibrium model of an isolated axisymmetric galaxy of roughly Milky Way mass. Their purpose was to create a simplified model of an isolated galaxy in which they could compare the performance of different codes, having different recipes for star formation and feedback. In order to ensure that the evolution of their model supported only mild spirals and avoided complications such as bar instabilities, they adopted a rather low mass disk, as shown in Fig. 1; at its peak, the fraction of central attraction from the disk, V_d^2/V_{tot}^2 , is about 1/3, making it what is known (Sackett 1997) as a strongly submaximum disk.

We have downloaded the “medium resolution” version of their model and evolved it using our GALAXY simulation code (Sellwood 2014). The supplied particle file has 1M disk “star” particles, 1M “gas” particles, 0.125M bulge particles, and 1M halo particles. The early evolution of the star (top row) and gas (bottom row) disk is displayed in Fig. 2, although in this simulation the “gas particles” were also treated as collisionless.

As expected for a low-mass disk, the spirals are multi-armed (Sellwood & Masters 2022), and the disk does avoid forming a bar. In the absence of full gas physics, the low random velocities of the gas particles, cause them to manifest filamentary spirals.

However, we here make a case that their model is not representative of real galaxies. We first note that more than 75% of spiral galaxies have 2- or 3-arm

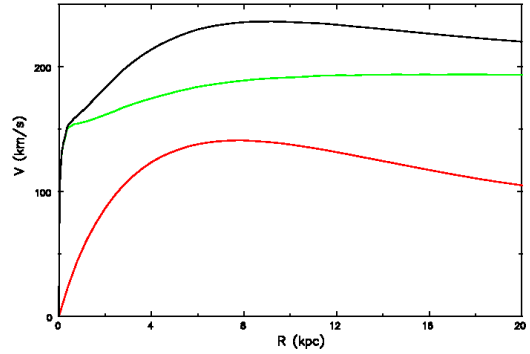


Figure 1. The black curve shows the rotation curve of the AGORA model. The red line shows the contribution from the disk star and “gas” particles and the green line the contribution from the bulge and halo. It is evident that this model has a strongly submaximal disk.

patterns (Davis et al. 2012; Hart et al. 2016; Yu & Ho 2018), making the evolution manifested in Fig. 2 quite untypical. Furthermore, multi-arm spiral patterns drive unrealistically slow dynamical evolution of the disk. The reasons for slow disk heating and radial migration in a submaximal disk are set out in the Appendix.

2. PROPOSED ALTERNATIVE MODEL

Here we propose an alternative disk+bulge+halo model that differs from the AGORA model by having a more massive disk in order that it will support fewer spiral arms, while the dense bulge component makes the model less prone to bar instabilities. The rotation curve of the equilibrium model is shown by the black curve in Fig. 3 and the separate contributions of the disk together with the bulge and halo, which are all realized with collisionless particles, are also shown. A similar model, with

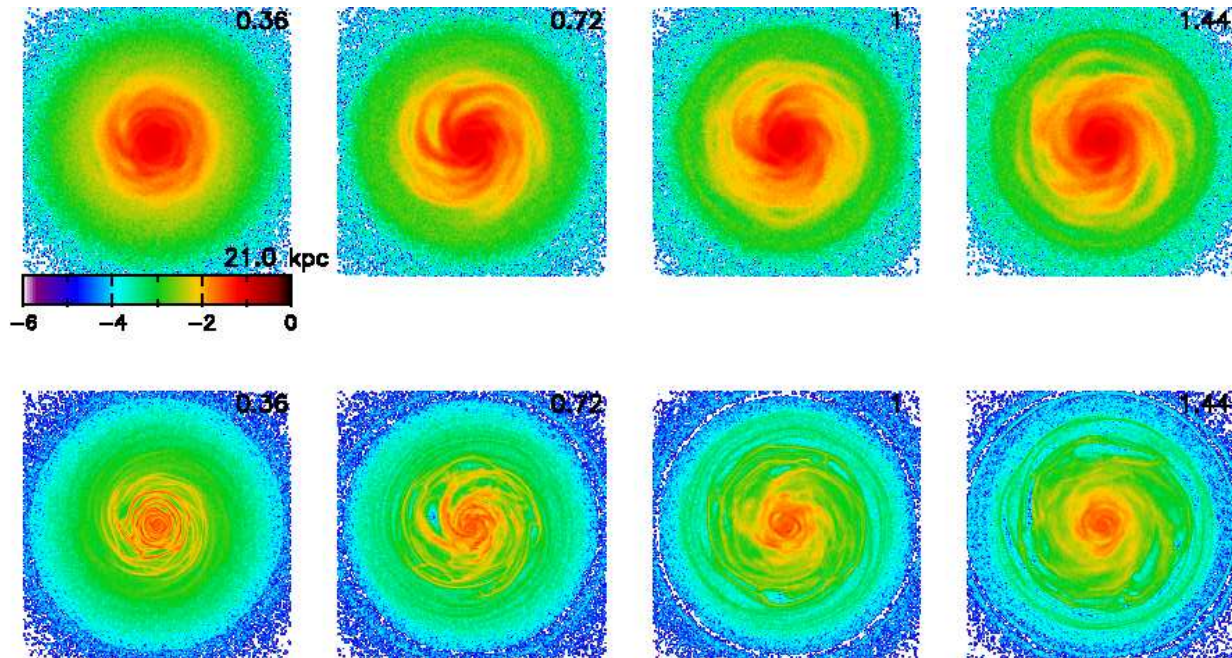


Figure 2. The evolution of the disk particle density in the “medium resolution” AGORA model. The color scale indicates the logarithm of the disk surface density. The top row shows the disk (star) particles, and the bottom the supplied gas particles, although here they are also treated as collisionless particles. The times are in Gyr and the box has a side of 42 kpc. Note the multi-arm nature of the spiral patterns that develop in the stellar disk (top row).

a bulge of slightly lower central density, was employed by Robinson et al. (2025).

2.1. Disk

The stellar disk is a thickened exponential with radial scale length R_d having the volume density

$$\rho_d(R, z) = \frac{M_d}{(2\pi)^{3/2} R_d^2} e^{-R/R_d} \exp\left(\frac{-z}{2z_0}\right)^2, \quad (1)$$

with z_0 being the constant disk scale height. We limit the radial extent of the disk by tapering the density (eq. 1) from its value at $R = 5.5R_d$ to zero at $R = 6R_d$, which discards a few percent of the mass. We assign velocities to the disk particles as described in §2.4 below.

2.2. Bulge

The spherical bulge has the cusped density profile proposed by Hernquist (1990)

$$\rho(r) = \frac{M_b a_b}{2\pi r (r + a_b)^3}, \quad (2)$$

with M_b being the bulge mass and a_b a scale radius. Hernquist also supplied an isotropic distribution function (DF) for this isolated mass distribution, which we employ in this composite model to set the bulge equilibrium, since the gravitational attraction in the center is dominated by the bulge.

2.3. Halo

We select a second, more extensive and massive spherical Hernquist model for the halo component, having mass M_h and radial scale a_h , and impose an outer boundary at $r = 5a_h$ to the otherwise infinite halo. Since the central attraction of the disk and bulge, which are embedded at the center of the halo, destroy the radial balance of the isotropic DF supplied by Hernquist, we must derive a revised equilibrium DF for the halo of the composite model.

Our method to achieve this is as follows: We start from the known isotropic DF for the halo with no embedded disk or bulge and compute its density change assuming that the masses of the disk and bulge were increased adiabatically from zero. As was pointed out by Young (1980), adiabatic changes to the total mass profile can be calculated semi-analytically, since the actions (Binney & Tremaine 2008) of the halo particles do not change as the potential well changes slowly; therefore the DF expressed as a function of the actions is the same after the adiabatic change as before.

Blumenthal et al. (1986) assumed angular momentum, one of the actions of an orbit, was alone conserved, but their formula would apply only if the orbits of all particles were initially and remained precisely circular. The orbits of particles in all reasonable spherical models librate radially, and therefore one must take conserva-

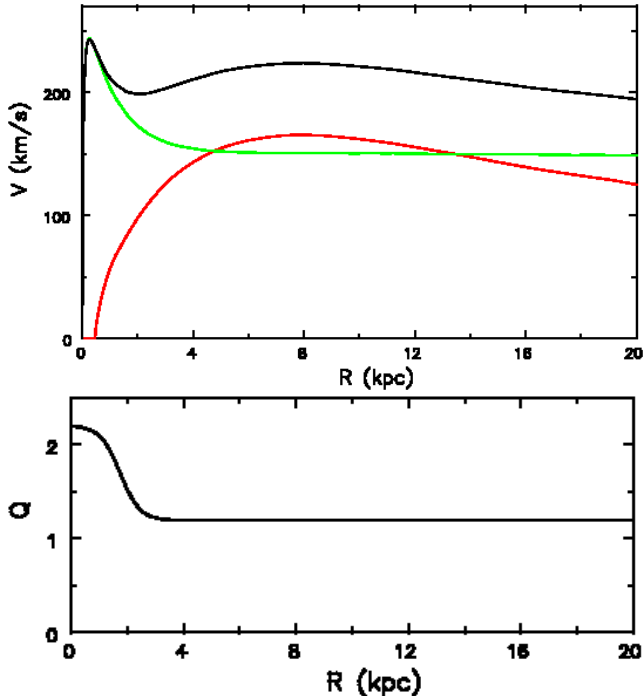


Figure 3. Upper panel: The black line gives the total rotation curve of this proposed model, after halo compression. The separate contributions of the thickened disk and the combined spherical bulge and halo are indicated by the red and green lines respectively. Lower panel: the initial radial dependence of Toomre’s Q .

tion of radial action into account when computing the density response to adiabatic changes to the potential, and the pressure of radial motions makes a realistic halo more resistant to compression than a naïve model with no radial action would predict.

Young (1980) and Sellwood & McGaugh (2005) describe procedures, which we employ here, to include radial action conservation, together with angular momentum conservation, as the potential well changes adiabatically. An initially isotropic DF becomes mildly radially biased, which can still be represented by the unchanged actions. Note that the procedure assumes the potential remains spherically symmetric, so we must approximate the disk potential by the monopole only term, *i.e.* the disk mass enclosed within a sphere of radius r . Sellwood & McGaugh (2005) found, from a comparison with a simulation in which a flat disk was grown slowly inside a spherical halo that the aspherical part of the disk potential caused negligibly small changes to the spherically averaged halo potential.

2.4. Disk particle velocities

We use the grid to solve for the initial gravitational attraction of the thickened disk (eq. 1), which we combine

Table 1. Proposed Milky Way model

Disk	mass	$M_d = 6.10 \times 10^{10} M_\odot$
	scalelength	$R_d = 3.5$ kpc
	vertical thickness	$z_0 = 350$ pc
	outer disk velocities	$Q = 1.2$
Bulge	mass	$M_b = 1.2 \times 10^{10} M_\odot$
	scale radius	$a_b = 245$ pc
	velocity distribution	isotropic
Initial halo	mass	$M_h = 1.2 \times 10^{11} M_\odot$
	scale radius	$a_h = 25$ kpc
	velocity distribution	see text

with that of the bulge and the now-known compressed halo density to obtain the gravitational field everywhere. We choose $Q = 1.2$ (Toomre 1964) over the outer disk, rising gently from $R = R_d$ to $Q = 2.2$ at the center as shown in the lower panel of Fig. 3 and select disk particles from the DF proposed by Shu (1969), with numerical details given in Sellwood (2014). The vertical velocities are set from the known density profile and potential, ignoring the small radial gradients.

2.5. Selection of parameters and scaling

Our choices for the parameters of the model are given in Table 1 which, after halo compression result in the rotation curve shown in Fig. 3. The disk is heavier than that in the AGORA model but at its peak $V_d^2/V_{\text{tot}}^2 \simeq 0.58$, which is still not fully maximal (Sackett 1997). We have scaled the model such that the unit of time $(R_d^3/GM_d)^{1/2} = 12.5$ Myr.

We can realize this model with any number of particles in each component, and find that it is reasonably close to equilibrium with $T/|W| \simeq 0.515$. Fig. 4 illustrates the first 3 Gyr of evolution of the disk, which is modeled by 1M star particles. There are no gas particles, but the bulge and halo (not shown) are represented by 0.1M and 1M particles respectively.

The disk supports bi-symmetric and 3-arm spiral patterns but does not form a bar. The evolution of models having ten times more and ten times fewer particles is quite similar.

2.6. Including gas

The model does not possess an explicit gas component. Users planning to implement gas physics based on particles, could simply relabel a fraction of the collisionless disk particles, selected at random (the particles are ordered by binding energy), as gas and assign them gas particle properties. Alternatively, for fluid-based gas physics, the mass of each disk particle can be reduced by the desired gas mass fraction, while implementing the fluid code. *e.g.* In the simulations reported

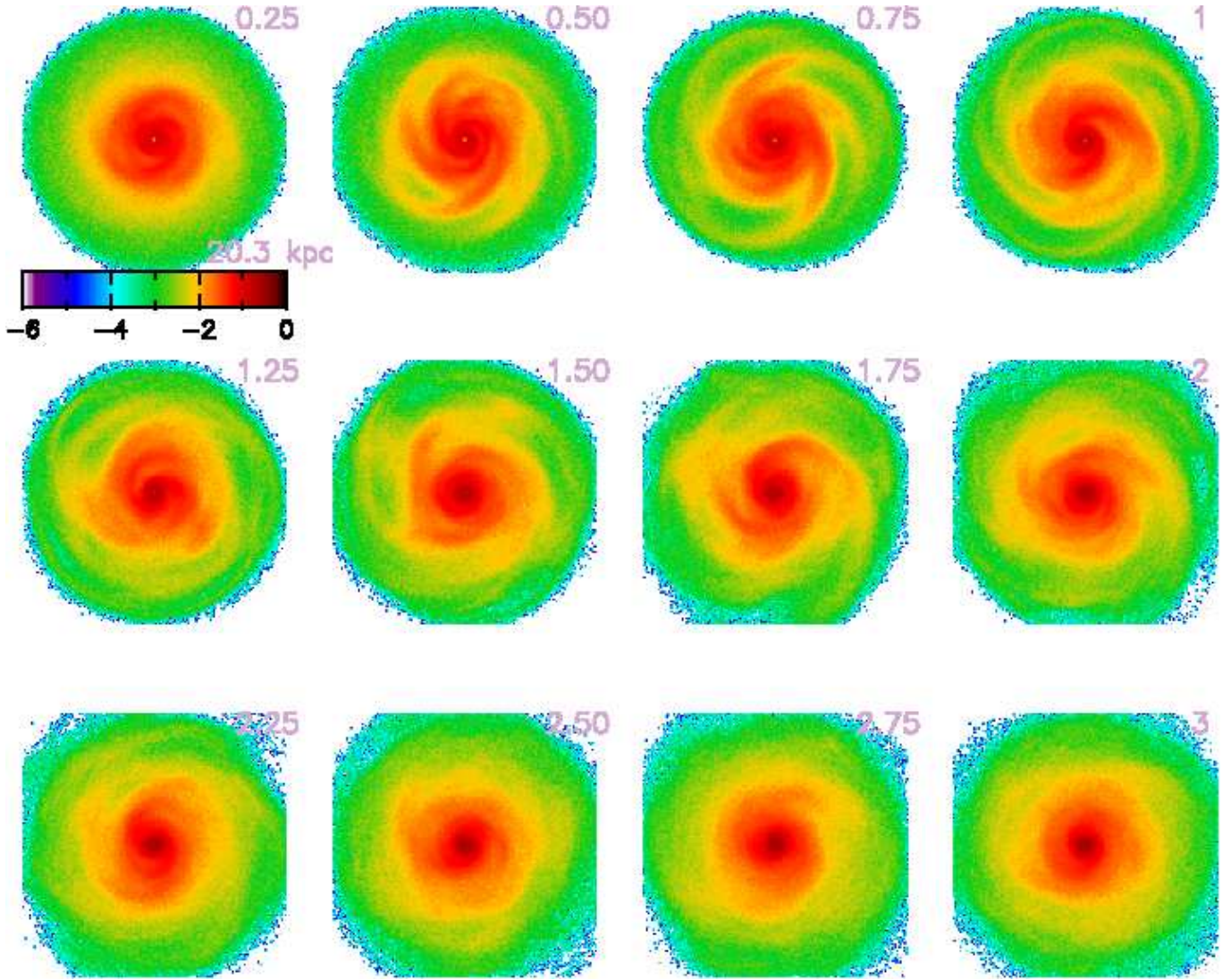


Figure 4. The first 3 Gyr of evolution of our proposed model having no gas component. The times are in Gyr and the half-widths of the frames are 20.3 kpc. Notice the strong, open spirals and the absence of a large bar.

by Robinson et al. (2025), we reduced the mass of each disk particle by 10% after 400Myr as the spiral patterns were beginning to develop, and replaced this mass by a gas component modeled by the RAMSES code (Teyssier 2002).

3. LOCATION AND FORMAT OF THE FILES

The website

<https://doi.org/10.25422/azu.data.30483479>

offers a choice of three versions of the same model each having a different number of particles:

- Low resolution model: 0.1M disk particles, 0.1M halo particles and 0.01M bulge particles
- Medium resolution model: 1M disk particles, 1M halo particles and 0.1M bulge particles

- High resolution model: 10M disk particles, 10M halo particles and 1M bulge particles

Having selected the version you want, you can download the appropriate gzipped tar ball and unpack it to obtain four files of ASCII data. The disk, halo, and bulge files tabulate coordinates of every particle in that component, one per line. The first three numbers are the (x, y, z) position in units of kpc, the next three are the (v_x, v_y, v_z) velocity in units of km/s, and the final number is the mass of the particle in units of 10^{10} solar masses. All particles within one component have the same mass, and the total mass of the model (*i.e.* the sum of the masses of all particles) is $\simeq 76 \times 10^{10}$ solar masses. The last small file, named `vcirc.dat`, is a table that gives the circular speed (in km/s) at 1000 ordered

radii (in kpc) to 50 kpc, and is included for reference only.

APPENDIX

The purpose of this appendix is to explain why multi-arm spirals heat a submaximal disk more slowly and support less radial migration than do patterns of greater scale in a heavier disk.

- Spirals extract energy from the gravitational well of the galaxy by outward transport of angular momentum, and the energy adds to the random motion of the stars. Sellwood & Binney (2002) showed, without approximation or invoking any particular spiral arm theory, that the change of radial action, ΔJ_R , of stars for a given quantity of angular momentum, ΔL_z , transported by a spiral pattern varies as

$$\Delta J_R = |\Delta L_z| / m, \quad (1)$$

where m is the angular periodicity, or number of arms in the pattern. This formula applies only at the Lindblad resonances where the increase is positive at both the inner and outer LRs even though the sign of the angular momentum change differs. The factor m in the denominator is because the radial extent of a spiral pattern is limited by its Lindblad resonances which are substantially closer to corotation for multi-arm patterns than for 2-arm spirals. Therefore, the efficiency of extraction of energy from the potential well by larger m spirals is reduced and the disk heats more slowly.

- Multi-arm patterns cause less radial migration (Sellwood & Binney 2002) for similar reasons. To summarize the mechanism, a growing spiral perturbation traps stars onto horseshoe orbits at corotation. As the amplitude rises, the width of the trapped region grows and trapped stars librate between the minima of the spiral potential where they reverse their motion in the rotating frame by gaining, or losing, angular momentum, which

causes them to move onto a new near circular path at a different radius. As the spiral decays, the trapped stars are released, and those that experienced an odd number (usually just one) of reversals while trapped will retain their new angular momenta, and therefore will have moved to orbits with greater, or smaller, guiding centers.

The consequences for multi-arm spirals are:

1. For a fixed spiral density amplitude, Σ_a in eq. (6.30) of Binney & Tremaine (2008), the perturbing potential is weaker for larger k (or shorter wavelength), which will diminish the radial extent of the horseshoe orbit region that is responsible for migration.
2. The period of a horseshoe orbit trapped in the CR depends on both its frequency difference from CR and the azimuthal distance between wave-crests, which is shorter for higher- m spirals. Since migration relies on the spiral having already decayed before a star makes its second horseshoe turn, those stars having periods long-enough to make only a single turn are confined to a narrower region about CR, implying a smaller average step size for migration.
3. The increased value of k causes the spiral potential to decay away from the mid-plane more rapidly, lessening its ability to affect the orbits of thick disk stars.

These factors, which stem from the short wavelength of the spirals, will reduce the extent of churning that is possible in both the thin and thick disks in simulations of atypically sub-maximum disks, as reported by Vera-Ciro et al. (2014). Note that Frankel et al. (2020) found strong evidence for copious migration by stars in the Milky Way.

REFERENCES

- Binney, J., & Tremaine, S. 2008, *Galactic Dynamics: Second Edition*
- Blumenthal, G. R., Faber, S. M., Flores, R., & Primack, J. R. 1986, *ApJ*, 301, 27, doi: [10.1086/163867](https://doi.org/10.1086/163867)
- Davis, B. L., Berrier, J. C., Shields, D. W., et al. 2012, *ApJS*, 199, 33, doi: [10.1088/0067-0049/199/2/33](https://doi.org/10.1088/0067-0049/199/2/33)
- Frankel, N., Sanders, J., Ting, Y.-S., & Rix, H.-W. 2020, *ApJ*, 896, 15, doi: [10.3847/1538-4357/ab910c](https://doi.org/10.3847/1538-4357/ab910c)

- Hart, R. E., Bamford, S. P., Willett, K. W., et al. 2016, MNRAS, 461, 3663, doi: [10.1093/mnras/stw1588](https://doi.org/10.1093/mnras/stw1588)
- Hernquist, L. 1990, ApJ, 356, 359, doi: [10.1086/168845](https://doi.org/10.1086/168845)
- Jung, M., Kim, J.-h., Nguyen, T. H., et al. 2025, arXiv e-prints, arXiv:2505.05720, doi: [10.48550/arXiv.2505.05720](https://doi.org/10.48550/arXiv.2505.05720)
- Kim, J.-h., Abel, T., Agertz, O., et al. 2014, ApJS, 210, 14, doi: [10.1088/0067-0049/210/1/14](https://doi.org/10.1088/0067-0049/210/1/14)
- Kim, J.-h., Agertz, O., Teyssier, R., et al. 2016, ApJ, 833, 202, doi: [10.3847/1538-4357/833/2/202](https://doi.org/10.3847/1538-4357/833/2/202)
- Robinson, H., Wadsley, J., Sellwood, J. A., & Pudritz, R. E. 2025, ApJ, 989, 205, doi: [10.3847/1538-4357/ade9c1](https://doi.org/10.3847/1538-4357/ade9c1)
- Sackett, P. D. 1997, ApJ, 483, 103, doi: [10.1086/304223](https://doi.org/10.1086/304223)
- Sellwood, J., & Masters, K. L. 2022, Annual Review of Astronomy and Astrophysics, 60, 73–120, doi: [10.1146/annurev-astro-052920-104505](https://doi.org/10.1146/annurev-astro-052920-104505)
- Sellwood, J. A. 2014, arXiv e-prints, arXiv:1406.6606, doi: [10.48550/arXiv.1406.6606](https://doi.org/10.48550/arXiv.1406.6606)
- Sellwood, J. A., & Binney, J. J. 2002, MNRAS, 336, 785, doi: [10.1046/j.1365-8711.2002.05806.x](https://doi.org/10.1046/j.1365-8711.2002.05806.x)
- Sellwood, J. A., & McGaugh, S. S. 2005, The Astrophysical Journal, 634, 70–76, doi: [10.1086/491731](https://doi.org/10.1086/491731)
- Shu, F. H. 1969, ApJ, 158, 505, doi: [10.1086/150214](https://doi.org/10.1086/150214)
- Teyssier, R. 2002, A&A, 385, 337, doi: [10.1051/0004-6361:20011817](https://doi.org/10.1051/0004-6361:20011817)
- Toomre, A. 1964, ApJ, 139, 1217, doi: [10.1086/147861](https://doi.org/10.1086/147861)
- Vera-Ciro, C., D’Onghia, E., Navarro, J., & Abadi, M. 2014, ApJ, 794, 173, doi: [10.1088/0004-637X/794/2/173](https://doi.org/10.1088/0004-637X/794/2/173)
- Young, P. 1980, ApJ, 242, 1232, doi: [10.1086/158553](https://doi.org/10.1086/158553)
- Yu, S.-Y., & Ho, L. C. 2018, ApJ, 869, 29, doi: [10.3847/1538-4357/aaeacd](https://doi.org/10.3847/1538-4357/aaeacd)